

**Quasinormal modes for the Vaidya metric**

Elcio Abdalla\* and Cecília B. M. H. Chirenti†

*Instituto de Física, Universidade de São Paulo, C.P. 66318, 05315-970—São Paulo, SP, Brazil*

Alberto Saa‡

*Departamento de Matemática Aplicada, UNICAMP, C.P. 6065, 13083-859—Campinas, SP, Brazil*

(Received 9 September 2006; published 25 October 2006)

We consider here scalar and electromagnetic perturbations for the Vaidya metric in double-null coordinates. Such an approach allows one to go a step further in the analysis of quasinormal modes for time-dependent spacetimes. Some recent results are refined, and a new nonstationary behavior corresponding to some sort of inertia for quasinormal modes is identified. Our conclusions can enlighten some aspects of the wave scattering by black holes undergoing some mass accretion processes.

DOI: [10.1103/PhysRevD.74.084029](https://doi.org/10.1103/PhysRevD.74.084029)

PACS numbers: 04.30.Nk, 04.40.Nr, 04.70.Bw

**I. INTRODUCTION**

The quasinormal modes (QNM) analysis is a paradigm for the study of gravitational excitations of black holes. For a comprehensive review of the vast previous literature, see [1,2]. We stress that the QNM of black holes are also experimentally relevant since they could, in principle, be detected in a gravitational waves detector such as LISA (see, for instance, [3] and references therein). The robustness of QNM analysis has been established by considering several kinds of generalizations, such as, for instance, relaxing the asymptotic flatness condition [4–6] or considering time-dependent situations [7–9]. The case of asymptotic anti-de Sitter black holes deserves special attention due to its relevance to the AdS/CFT conjecture [10–22].

The analysis of QNM for time-dependent situations is of special physical interest since it is expected that a black hole can enlarge its mass by some accretion process, or even lose mass by some other process, including Hawking radiation. The late time tail for a Klein Gordon field under a time-dependent potential was first considered in [7], where some influence of the temporal dependence of the potential over the characteristic decaying tails was reported. Such a kind of time-dependent potential arises naturally when the Vaidya metric is considered [8,9]. The Vaidya metric, which in radiation coordinates  $(w, r, \theta, \phi)$  has the form

$$ds^2 = -\left(1 - \frac{2m(w)}{r}\right)dw^2 + 2cdrdw + r^2d\Omega^2, \quad (1)$$

where  $d\Omega^2 = d\theta^2 + \sin^2\theta d\phi^2$ ,  $c = \pm 1$ , is a solution of Einstein's equations with spherical symmetry in the eikonal approximation to a radial flow of unpolarized radiation. For the case of an ingoing radial flow,  $c = 1$  and  $m(w)$  is a monotone increasing mass function in the advanced time  $w$ , while  $c = -1$  corresponds to an outgoing radial flow,

with  $m(w)$  being, in this case, a monotone decreasing mass function in the retarded time  $w$ . The metric (1) is the starting point for the QNM analysis of varying mass black holes.

In [9], massless scalar fields were studied on an electrically charged version of the Vaidya metric. Basically, two kinds of continuously varying mass functions were considered:

$$m(w) = \begin{cases} m_1 & w \leq w_1, \\ m_1 f(w) & w_1 \leq w \leq w_2, \\ m_2 & w \geq w_2, \end{cases} \quad (2)$$

with  $f(w) = (1 - \lambda w)$  and  $f(w) = \exp(-\alpha w)$ , called, respectively, linear and exponential models. Generalized tortoise coordinates were introduced, and a standard numerical analysis was done. The conclusion was that, as a first approximation, the QNM for a stationary Reissner-Nordström black hole with mass  $m(w)$  and charge  $q(w) = q_0 m(w)$  are still valid, as if some stationary adiabatic regime was indeed governing the QNM dynamics for time-dependent spacetimes. In principle, one should not expect such stationary behavior for very rapidly varying mass functions; however, the analysis of [9] was not able to identify any breaking of such an adiabatic regime. We notice also that both linear and exponential models, inspired by some known exact solutions [23] for which generalized tortoise coordinates could be explicitly constructed, would hardly correspond to physically realistic cases. Both cases have  $C^0$ -class mass functions, implying the existence of some infinitesimal shell distributions of matters for  $w = w_0$  and  $w = w_1$  whose interpretation and role are still unclear.

We attack here the QNM problem by considering the Vaidya metric in double-null coordinates [24]. The main advantage of such an approach is the possibility of considering any (monotone) mass function, allowing, for instance, the analysis of smooth mass functions that could correspond to physically more relevant situations, free of obscure infinitesimal matter shells. Furthermore, the use of

\*Electronic address: eabdalla@fma.if.usp.br

†Electronic address: cecilia@fma.if.usp.br

‡Electronic address: asaa@ime.unicamp.br

double-null coordinates has improved considerably the overall precision of the numerical analysis, allowing us to identify the breakdown of the adiabatic regime, characterized by the appearance of a nonstationary inertial effect for the QNM in the case of rapidly varying mass functions. Once the stationary regime is reached, the standard QNM results hold, reinforcing, once more, the robustness of the QNM analysis. Our results can be used as a first approximation to describe the propagation of small perturbations around astrophysically realistic situations where black holes undergo some mass accretion processes. We notice that the nonstationary inertial effect presented here is in perfect agreement with the nonlinear analysis performed in [25], which reported extra redshift effects on the QNM frequencies due to the growth of the effective black hole mass.

We organize this paper as follows. The next section is devoted to a brief introduction of the semianalytical approach [24] for the Vaidya metric in double-null coordinates. Section III presents the main issues and results of our numerical analysis. The last section contains some closing remarks.

## II. THE VAIDYA METRIC IN DOUBLE-NULL COORDINATES

Double-null coordinates are specially suitable for time-evolution problems such as the QNM analysis. However, the difficulties of constructing double-null coordinates for nonstationary spacetime are well known. The Vaidya metric is a typical example (see [24] and references therein). Indeed, it is known that the problem of constructing double-null coordinates for generic mass functions is not analytical soluble in general [23]. The semianalytical approach proposed in [24] is the starting point for our analysis here. It consists, basically, of considering the Vaidya metric in double-null coordinates *ab initio*, avoiding the need for constructing any coordinate transformation. The spherically symmetric line element in double-null coordinates is

$$ds^2 = -2f(u, v)dudv + r^2(u, v)d\Omega^2, \quad (3)$$

where  $f(u, v)$  and  $r(u, v)$  are smooth nonvanishing functions. The energy-momentum tensor of a unidirectional radial flow of unpolarized radiation in the eikonal approximation is given by

$$T_{ab} = \frac{1}{8\pi} h(u, v) k_a k_b, \quad (4)$$

where  $k_a$  is a radial null vector. Einstein's equations for the case of a flow in the  $v$  direction can then be reduced to the following set of equations [23,24]:

$$f(u, v) = 2B(v)\partial_u r(u, v), \quad (5)$$

$$\partial_v r(u, v) = -B(v)\left(1 - \frac{2m(v)}{r(u, v)}\right), \quad (6)$$

$$h(u, v) = -4\frac{B(v)m'(v)}{r^2(u, v)}, \quad (7)$$

where  $B(v)$  and  $m(v)$  are arbitrary functions obeying, according to the weak energy condition,

$$B(v)m'(v) \leq 0, \quad (8)$$

where the prime denotes the derivative with respect to  $v$ . The solution of (5)–(7) will correspond to the Vaidya metric in double-null coordinates, as one can interpret from (3) and (4). For  $m'(v) \neq 0$ , the choice

$$B = -\frac{1}{2} \text{sign}(m') \quad (9)$$

allows one to interpret  $m(v)$  as the mass of the solution and  $v$  as the proper time as measured in the rest frame at infinity for the asymptotically flat case [23,24]. Note that, if the weak energy condition (8) holds, the function  $m(v)$  is monotone, implying that the radial flow must be ingoing or outgoing for all  $v$ . It is not possible, for instance, to have “oscillating” mass functions  $m(v)$ .

The semianalytical approach of [24] consists of a strategy to construct numerically the functions  $f(u, v)$ ,  $r(u, v)$ , and  $h(u, v)$  from Eqs. (5)–(7), and to infer the underlying causal structure. Equation (6) along the lines of constant  $u$  is a first order ordinary differential equation in  $v$ . One can evaluate the function  $r(u, v)$  at any point by solving the  $v$ -initial value problem knowing  $r(u, v_0)$ . The trivial example of Minkowski spacetime ( $m = 0$ ), for instance, can be obtained [24] by choosing  $r(u, 0) = u/2$ . Once we have  $r(u, v)$ , we can evaluate  $f(u, v)$  and  $h(u, v)$  from (5) and (7). Further details of the method can be found in [24]. We consider here the following smooth mass function:

$$m(v) = m_1 + \frac{m_2 - m_1}{2} [1 + \tanh\rho(v - v_1)] \quad (10)$$

where  $\rho$  and  $v_1$  are also constant parameters. For the sake of comparison with the results of [9], we also consider a linear model. Figure 1 depicts the causal structure corresponding to the hyperbolic mass function (10) obtained from the semianalytical approach. For positive  $\rho$  and  $m_2 > m_1$ , for instance, it represents a black hole with mass  $m_1$  receiving a radial flux of radiation and, consequently, enlarging continuously its mass until reaching  $m_2$ . The choice of the initial condition for solving (6) is a rather subtle issue [24]. For our purposes here, we note only that demanding  $\partial_u r(u, v_0) \neq 0$  is sufficient to guarantee that, for any  $m(v)$ , the underlying spacetime causal structure does not depend on the initial condition  $r(u, v_0)$ . For constant  $m$  and  $B = -1/2$ , Eq. (6) can be easily integrated, leading to

$$r(u, v) + 2m \ln|r(u, v) - 2m| - \frac{v}{2} = P(u), \quad (11)$$

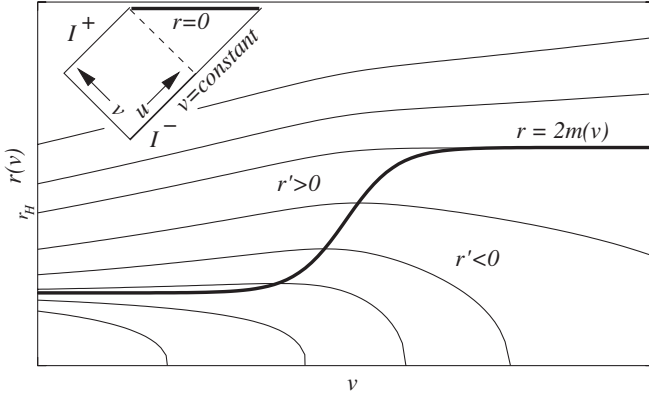


FIG. 1. Lines of constant  $u$  for the solution of (6) with the hyperbolic mass function (10), with  $m_2 > m_1$  and  $\rho > 0$ . All solutions in the region below the line  $r = 2m(v)$  (the apparent horizon) have  $r' < 0$ , where the prime denotes the derivative with respect to  $v$ . Any solution that enters into this region will reach the singularity at  $r = 0$  with finite  $v$ . On the other hand, solutions confined to the  $r' > 0$  region always escape from the singularity and reach  $I^+$ . In the present case, there exists an event horizon (the dashed line in the inserted conformal diagram) close to the solutions  $r_H(v)$ .

where  $P(u)$  is an arbitrary function of  $u$ . It is also possible to solve Eq. (6) analytically for the linear and exponential mass functions [23]. Equation (11) is our reference to choose the initial conditions  $r(u, v_0)$ .

### III. SCALAR AND ELECTROMAGNETIC PERTURBATIONS

In the coordinate system (3), for any desired form of the mass function  $m(v)$ , the equations for scalar and electromagnetic perturbations can be easily put in the form [2]

$$\frac{\partial^2 \psi}{\partial u \partial v} + V(u, v) f(u, v) \psi = 0, \quad (12)$$

where the potential  $V(u, v)$  is given by

$$V(u, v) = \frac{\ell(\ell + 1)}{2r^2(u, v)} + \sigma \frac{m(v)}{r^3(u, v)}, \quad (13)$$

where  $\sigma = 1$  and  $\sigma = 0$  correspond, respectively, to the scalar and to the electromagnetic cases. For a given mass function  $m(v)$ , one first evaluates the functions  $f(u, v)$  and  $r(u, v)$  with the semianalytical approach of the previous section, and then the characteristic problem corresponding to (12) can be solved with the usual second order characteristic algorithm [2], where the initial data are specified along the two null surfaces  $u = u_0$  and  $v = v_0$ . Since the basic aspects of the field decay are independent of the initial conditions (this fact is confirmed by our simulations), we use the Gaussian initial condition

$$\psi(u = u_0, v) = \exp\left[-\frac{(v - v_c)^2}{2\sigma^2}\right], \quad (14)$$

and  $\psi(u, v = v_0) = \text{const}$ . Our typical numerical grid is large enough to assure that we can set effectively this last constant to zero. After the integration is completed, the values  $\psi(u_{\text{max}}, v)$  are extracted, where  $u_{\text{max}}$  is the maximum value of  $u$  on the numerical grid. Taking sufficiently large  $u_{\text{max}}$ , we have good approximations for the wave function at the event horizon. Figure 2 presents an example of  $\psi(u_{\text{max}}, v)$  data for a hyperbolic increasing mass function and its comparison with the case of a Schwarzschild black hole. Similar results hold if we extract the data for other values of  $u$ . All the analysis presented here corresponds to the data extracted on the horizon  $u_{\text{max}}$ . Note that the choice of  $u_{\text{max}}$  is a matter of numerical convenience. Since the QNM corresponds to eigenstates of an effective Schroedinger equation [2], the associated complex eigenvalues can be read out anywhere once the asymptotic regime is attained.

From the function  $\psi(u_{\text{max}}, v)$ , one can infer the characteristic frequencies  $\omega$  of the damped oscillating modes. Since the frequencies  $\omega$  are themselves time dependent (see Fig. 2), for a given  $v$ ,  $\omega(v)$  is determined locally by a nonlinear  $\chi^2$ -fitting by using some damped cycles of  $\psi$  around  $v$ . We perform an exhaustive numerical analysis for many different mass functions  $m(v)$ . Figures 3 and 4 present the real ( $\omega_R$ ) and imaginary ( $\omega_I$ ) parts of the frequencies of the perturbations as a function of  $v$ . They correspond, respectively, to some decreasing and increasing mass functions, and are typical for all values of  $\ell$ , all kinds of perturbations (scalar and electromagnetic), and different initial conditions. The imaginary part  $\omega_I$  exhibits similar time dependence, although its values are typically known with lower precision than  $\omega_R$ . This is not, however, due to numerical errors in the integration procedure. In

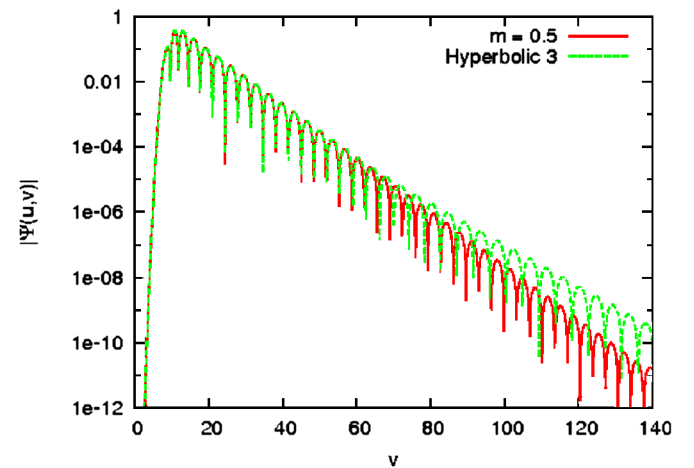


FIG. 2 (color online). Values of the electromagnetic perturbations  $\psi(u_{\text{max}}, v)$  with  $\ell = 2$  for a Schwarzschild black hole with mass  $m = 0.5$  and for the Vaidya metric with the hyperbolic mass function (10), where  $v_1 = 75$ ,  $\rho = 0.08$ ,  $m_1 = 0.5$ , and  $m_2 = 0.65$  (Hyperbolic 3). One can clearly appreciate, for the time-dependent case, the slowing down of the oscillation frequency and damping taking place after  $v_1$ .

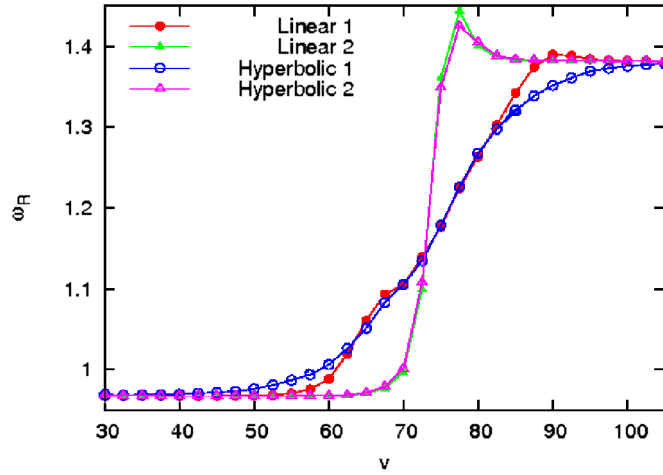


FIG. 3 (color online). The real ( $\omega_R$ ) part of the frequency for scalar perturbations with  $\ell = 2$  as a function of  $\nu$  for decreasing linear and hyperbolic mass functions. For all the cases,  $m_1 = 0.5$  and  $m_2 = 0.35$ . Linear 1:  $\nu_1 = 60$ ,  $\nu_2 = 90$ . Linear 2:  $\nu_1 = 74.5$ ,  $\nu_2 = 75.5$ . Hyperbolic 1:  $\nu_1 = 75$ ,  $\rho = 0.08$ . Hyperbolic 2:  $\nu_1 = 75$ ,  $\rho = 0.8$ . The imaginary part  $\omega_I$  has similar behavior for the increasing mass case (Fig. 4); see the text.

fact, the convergence of the second order characteristic algorithm is quite good. For instance, the differences in the calculated frequencies of Figs. 3 and 4, obtained by using as integration steps  $\Delta u = \Delta v = 0.2, 0.1$ , and  $0.05$ , are smaller than the size of the points used in the figures, and no difference is detected for even smaller steps. We credit the irregularities observed for  $\omega_I$  to the local  $\chi^2$ -fitting described above. For subcritical damped oscillations such as the QNM considered here, the oscillation frequencies  $\omega_R$  can be easily determined from a few damped cycles, while for the damping term  $\omega_I$  one typically needs many more cycles in order to get a similar precision. By taking a large number of cycles, we will tend to smear the calculated frequencies, leading to some kind of average and not to the desired instantaneous values. We opt, then, to take as few as possible cycles, paying the price of having some irregularities for  $\omega_I$ .

Let us consider for a close analysis, for instance, the case of decreasing  $m(v)$  (Fig. 3). For the rapidly varying cases (Linear 2 and Hyperbolic 2), one clearly sees the inertial effect for  $\omega_R$  near  $\nu = 75$ . The function  $\omega_R(v)$  does not follow the track corresponding to  $m^{-1}(v)$ , as one would expect for a stationary adiabatic regime, and as it really does for the Hyperbolic 1 case. After the rapidly increasing phase,  $\omega_R$  behaves as if it would have some intrinsic inertia, reaching a maximum value that is bigger than  $\omega_R(\infty)$ , implying the relaxation corresponding to the region with  $\omega'_R(v) < 0$  for  $\nu > 75$ . We also notice that, for the rapidly varying case, one could not detect sensible differences between the smooth hyperbolic case and the  $C^0$  linear one. Nevertheless, one can see that the slower linear case (Linear 1) exhibits some inertial effects close to

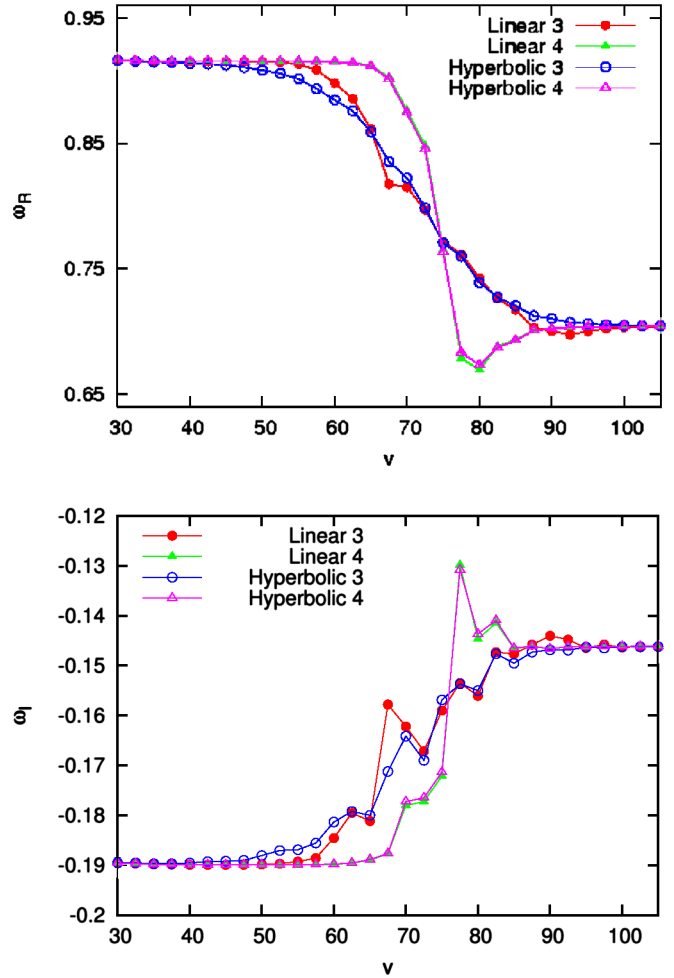


FIG. 4 (color online). The real ( $\omega_R$ ) and imaginary ( $\omega_I$ ) parts of the frequency for electromagnetic perturbations with  $\ell = 2$  as a function of  $\nu$  for increasing linear and hyperbolic mass functions. For all the cases,  $m_1 = 0.5$  and  $m_2 = 0.65$ . Linear 3:  $\nu_1 = 60$ ,  $\nu_2 = 90$ . Linear 4:  $\nu_1 = 74.5$ ,  $\nu_2 = 75.5$ . Hyperbolic 3:  $\nu_1 = 75$ ,  $\rho = 0.08$ . Hyperbolic 4:  $\nu_1 = 75$ ,  $\rho = 0.8$ .

the second matching point of  $m(v)$ . In all other regions, it follows the track corresponding to  $m^{-1}(v)$ . No appreciable difference in the transients of scalar and electromagnetic perturbations was detected. As we have already mentioned, such transient inertial behavior could not be detected by the QNM analysis done in radiation coordinates presented in [9]. Analogous conclusions hold for the case of increasing  $m(v)$  (Fig. 4). In fact, since the increasing mass functions considered here can be obtained from the decreasing ones by a time reversal  $m(v) \rightarrow m(-v)$ , the underlying causal structures are equivalent [24], and the corresponding QNM are also related. Under a time reversal, the graph of  $\omega_R$  (and of  $\omega_I$ ) must be reflected on a horizontal axis.

We could infer from our numerical simulations the situation corresponding to the onset of the QNM nonstationary inertial behavior. The deviation from the stationary regime is measured by the second derivative of the mass

function  $m''(\nu)$ . Heuristically, one should expect the appearance of nonstationary behavior when  $|1/m''|$  is smaller than a certain characteristic time of the system, which should prevent the system from relaxing into an adiabatic regime. There are two characteristic times associated with the QNM of black holes: the oscillation period  $2\pi/\omega_R$  and the damping time  $|1/\omega_I|$ . The onset of the inertial behavior is associated with the second one. We verify appreciable deviations from the stationary regime whenever  $|m''(\nu)|$  is of the same order (or larger) than  $|\omega_I|$ . For instance, for Hyperbolic 2 and Hyperbolic 4 data sets (corresponding to the inertial behavior depicted in Figs. 3 and 4) we have  $|m''_{\max}/\omega_I^{\text{final}}| \approx 25\%$ , while for Hyperbolic 1 and Hyperbolic 3 (the stationary behavior) such a ratio is 100 times smaller. Estimating the magnitude of the inertial effect from our numerical simulations without an approximated analytical model seems to be much harder. Again heuristically, one expects the magnitude of the effect to be proportional to  $|m''|\tau$ , where  $\tau$  is the time interval along which  $|m''| \gtrsim |\omega_I|$ . We could check that the relative variations in frequencies during the inertial behavior for the smooth case are always limited by the ratio  $|m''/\omega_I|$ . Further analytical work is certainly necessary to enlighten this point. We finish by noticing that, for the  $C^0$  linear case,  $|m''_{\max}|$  is always large, increasing indeed with  $1/\Delta\nu$ , and hence nonstationary inertial behavior is reported in all simulations using the  $C^0$  linear data set. Since  $\tau$  is very small in such cases (of the same order as  $\Delta\nu$ ), the magnitude of the inertial effects is also typically small.

#### IV. FINAL REMARKS

All situations we considered in the present work involve mass functions corresponding to an initial black hole with mass  $m_1$  undergoing some mass accretion or decrease process and ending with a mass  $m_2$ . Such an ‘‘asymptotic Schwarzschild’’ choice assures us that the spacetime has the usual black hole causal structure for  $\nu \rightarrow \pm\infty$  and, consequently, that QNM can be defined in the usual way and that the corresponding frequencies can be properly compared. For all the cases considered, the inertial transients dissipate away and  $\omega(\nu)$  tends to follow the track of  $m^{-1}(\nu)$  rather quickly, confirming the robustness of the numerical QNM analysis. The integration in double-null coordinates has turned out to be much more efficient than the integration in radiation coordinates [9], allowing us to reach the precision necessary to unveil the reported nonstationary behavior with quite modest computational resources. Despite the fact that radiation coordinates are known to be defective at the horizon [26], we believe that numerical analyses such as those presented in [9] are still confident since the QNM analysis is always concerned

with the exterior region of the black hole. However, as confirmed by the present calculations, algorithms based on the characteristic integration are typically more efficient by far.

An interesting extension of this work would be the analysis of the highly damped QNM (overtones,  $n > 0$ ). Since for such overtones the ratio  $|\omega_I/\omega_R|$  is always larger than for the  $n = 0$  QNM considered here, including, for sufficiently large  $n$ , cases for which  $|\omega_I/\omega_R| > 1$ , it would be interesting to check if the nonstationary inertial behavior could somehow be attenuated for  $n > 0$ . We notice that the numerical analysis presented here cannot be extended directly to the  $n > 0$  case since one cannot identify the  $n > 0$  frequencies with sufficient accuracy. We believe this could be attained, in principle, by means of the WKB approximation.

Although the typical astrophysical situations of mass accretion for black holes will hardly keep spherical symmetry intact during intermediate stages, our results can be used as a first approximation for the scattering by these sources since, as it is well known, after the transient phases, the system should accommodate itself in a stationary spherical symmetric configuration. One must, however, keep in mind that nonstationary inertial behavior in the QNM frequencies is expected to take place whenever  $|m''| \gtrsim |\omega_I|$ , rendering the analysis of the rapidly varying situations a subtler task.

The evaporation by Hawking radiation could indeed be considered as a physically genuine process where the black hole mass decreases and spherical symmetry is maintained. Our approach can be applied to this case, with some crucial remarks about the causal structure of the spacetime left behind after the evaporation [27].

We finish by noticing, as it is well known, that the damped oscillations correspond to an intermediate phase in the wave scattering by asymptotically flat black holes. The very last final phase corresponds, indeed, to a power law decay. In the problems considered here, the power law tail typically appears for large values of  $\nu$  for which the QNM already settled down in the stationary phase, with no trace from the transients. We do not detect, in this case, any influence of the time dependence of the potential in these tails. There is no contradiction with the results reported in [7]. This is a consequence of our choice of ‘‘asymptotic Schwarzschild’’ mass functions, for which the corresponding potential has no resemblance to the ones considered in [7].

#### ACKNOWLEDGMENTS

The authors are grateful to FAPESP and CNPq for financial support.

- [1] H. P. Nollert, *Classical Quantum Gravity* **16**, R159 (1999).
- [2] K. D. Kokkotas and B. G. Schmidt, *Living Rev. Relativity* **2**, 2 (1999).
- [3] E. Berti, V. Cardoso, and C. M. Will, *Phys. Rev. D* **73**, 064030 (2006).
- [4] P. R. Brady, C. M. Chambers, W. Krivan, and P. Laguna, *Phys. Rev. D* **55**, 7538 (1997); P. R. Brady, C. M. Chambers, W. G. Laarakkers, and E. Poisson, *Phys. Rev. D* **60**, 064003 (1999).
- [5] C. Molina, D. Giugno, E. Abdalla, and A. Saa, *Phys. Rev. D* **69**, 104013 (2004).
- [6] D. P. Du, B. Wang, and R. K. Su, *Phys. Rev. D* **70**, 064024 (2004); E. Abdalla, B. Wang, A. Lima-Santos, and W. G. Qiu, *Phys. Lett. B* **538**, 435 (2002); E. Abdalla, K. H. C. Castello-Branco, and A. Lima-Santos, *Phys. Rev. D* **66**, 104018 (2002).
- [7] S. Hod, *Phys. Rev. D* **66**, 024001 (2002).
- [8] L. H. Xue, Z. X. Shen, B. Wang, and R. K. Su, *Mod. Phys. Lett. A* **19**, 239 (2004).
- [9] C. G. Shao, B. Wang, E. Abdalla, and R. K. Su, *Phys. Rev. D* **71**, 044003 (2005).
- [10] J. S. F. Chan and R. B. Mann, *Phys. Rev. D* **55**, 7546 (1997); **59**, 064025 (1999).
- [11] V. Cardoso and J. P. S. Lemos, *Phys. Rev. D* **63**, 124015 (2001).
- [12] G. T. Horowitz and V. E. Hubeny, *Phys. Rev. D* **62**, 024027 (2000).
- [13] B. Wang, C. Y. Lin, and E. Abdalla, *Phys. Lett. B* **481**, 79 (2000).
- [14] B. Wang, C. Molina, and E. Abdalla, *Phys. Rev. D* **63**, 084001 (2001).
- [15] V. Cardoso and J. P. S. Lemos, *Phys. Rev. D* **64**, 084017 (2001); *Classical Quantum Gravity* **18**, 5257 (2001).
- [16] E. Berti and K. D. Kokkotas, *Phys. Rev. D* **67**, 064020 (2003).
- [17] R. A. Konoplya, *Phys. Rev. D* **66**, 044009 (2002).
- [18] D. Birmingham, I. Sachs, and S. N. Solodukhin, *Phys. Rev. Lett.* **88**, 151301 (2002); D. Birmingham, *Phys. Rev. D* **64**, 064024 (2001).
- [19] J. M. Zhu, B. Wang, and E. Abdalla, *Phys. Rev. D* **63**, 124004 (2001); B. Wang, E. Abdalla, and R. B. Mann, *Phys. Rev. D* **65**, 084006 (2002); B. Wang, C. Y. Lin, and C. Molina, *Phys. Rev. D* **70**, 064025 (2004).
- [20] S. Musiri and G. Siopsis, *Phys. Lett. B* **576**, 309 (2003); R. Aros, C. Martinez, R. Troncoso, and J. Zanelli, *Phys. Rev. D* **67**, 044014 (2003); A. Nunez and A. O. Starinets, *Phys. Rev. D* **67**, 124013 (2003); E. Winstanley, *Phys. Rev. D* **64**, 104010 (2001).
- [21] V. Cardoso and J. P. S. Lemos, *Phys. Rev. D* **67**, 084020 (2003).
- [22] V. Cardoso, R. Konoplya, and J. P. S. Lemos, *Phys. Rev. D* **68**, 044024 (2003).
- [23] B. Waugh and K. Lake, *Phys. Rev. D* **34**, 2978 (1986).
- [24] F. Giroto and A. Saa, *Phys. Rev. D* **70**, 084014 (2004).
- [25] Y. Zlochower, R. Gomez, S. Husa, L. Lehner, and J. Winicour, *Phys. Rev. D* **68**, 084014 (2003).
- [26] R. Lindquist, R. Schwartz, and C. Misner, *Phys. Rev.* **137**, B1364 (1965).
- [27] E. Abdalla, C. B. M. H. Chirenti, and A. Saa (unpublished).